Supporting Information

Sequence elements that uncouple R-loop formation and stability in CRISPR-Cas systems

Mark D. Szczelkun, Maria S. Tikhomirova, Tomas Sinkunas, Giedrius Gasiunas, Tautvydas Karvelis, Patrizia Pschera, Virginijus Siksnys, Ralf Seidel

SI Materials and Methods

DNA

All DNA constructs were based on pUC18 or pUC19 plasmids into which single protospacer/PAM elements were inserted via the EcoRI or SmaI sites, respectively (see Tables S2 and S3 for the details). For preparing constructs for the tweezers experiments, a ~2.1 kbp fragment containing a single protospacer/PAM combination was made by PCR from the recombinant plasmids (see Table S4 for primer sequences), digested with NotI and SpeI and purified. Biotin- or digoxigenin-modified attachment handles were made using 1.2 kbp (Cascade) or 1.0 kbp (Cas9) DNA fragments that where labelled with biotin- or digoxigenin-dUTP by PCR (see Table S4 for primer sequences), and which were digested with either NotI or SpeI. The protospacer fragment was ligated with the biotin/dig-labelled handles using T4 DNA ligase. For the Cascade DNA, the full ligation product was purified from agarose gels preventing any exposure to EtBr and UV light (1,2).

Production of Cascade and Cas9-crRNA-tracrRNA complexes

The Cascade complex was purified from the *E. coli* cells as described previously (3).
To obtain Cascade lacking the CasA subunit (Cascade-ΔCasA), *casDE* (*cse5-cas6e*) and *casBC* (*cse2-cas7*) gene cassettes were cloned into the modified version of the pCDF-Duet1 plasmid (Novagen) which contains the His-tag sequence instead of the S-tag. *E.coli* BL21 (DE3) cells were cotransformed with the resulting recombinant pCascadeΔA plasmid and pCRh (Sinkunas et al, 2013). Cells were grown in LB broth (BD) supplemented with chloramphenicol (17 μg/ml), and streptomycin (25 μg/ml) at 37°C to OD_{600nm} of ~ 0.5. The Cascade-ΔCasA complex expression was induced with 1 mM IPTG for 3 h. Harvested cells were disrupted by sonication and cell debris removed by centrifugation. The Cascade-ΔCasA complex was purified by Ni^{2+}-affinity, size exclusion and heparin-affinity chromatography as described (3). To obtain the CasA protein, the *casA* (*cse1*) gene was cloned into pBAD24-CHis expression vector via NcoI and XhoI sites to generate a pCasA plasmid. CasA was expressed in *E. coli* BL21 (DE3) cells grown in LB broth supplemented with ampicillin (50 μg/ml). Cells were grown at 37°C to OD_{600nm} of ~ 0.7 and expression induced with 0.2% (w/v) arabinose for 3 h. Harvested cells were disrupted by sonication and cell debris were removed by centrifugation. The supernatant was loaded onto the Ni^{2+}-charged HiTrap chelating HP column (GE Healthcare) and eluted with a linear gradient of increasing imidazole. The fractions containing CasA were pooled and subsequently loaded onto Superdex 200 (HiLoad 16/60; GE Healthcare) column. Both the Cascade and Cascade-ΔCasA complexes and the CasA protein were stored at -20°C in a buffer containing 20 mM Tris–HCl (pH 8), 500 mM NaCl, 50% (v/v) glycerol.
The Cas9-crRNA-tracrRNA complex was assembled *in vitro* as described (4). Briefly, His_6-tagged Cas9 protein was mixed with a pre-annealed crRNA and tracrRNA duplex at 1:1 molar ratio and incubated in Buffer SB (10 mM Tris-HCl, pH 7.5 at 37°C, 100 mM NaCl, 0.1 mM DTT and 5 μg/ml BSA) at 37°C for 1 h. The 42 nt crRNA (5′-CGCUAAAGAGGAAGAGGACAGUUUUAGAGCUGUGUUGUUUCG-3′) was obtained from

Metabion (Martinsried, Germany), while the 78-nt tracrRNA was produced by *in vitro* transcription using TranscriptAid T7 High Yield Transcription Kit (Thermo Fisher Scientific) as described (4).

Single-molecule observation of R-loop formation

Single-molecule experiments with Cascade and Cas9 were carried out as previously described (5,6) using magnetic tweezers setups that were, respectively, a home-built (7) instrument (equipped with a Pulnix 1067CL CCD camera, image acquisition at 120 Hz) or a commercial instrument (Picotwist, Saint Romain de Popey, France, equipped with a Jai CV-A10 GE camera, image acquisition at 60 Hz). The fluidic cells for the Cascade experiments were constructed from a polystyrene-coated and an uncoated 24x60 mm coverslip (Menzel-Gläser No. 1) and a Parafilm spacer. The fluidic cells for the Cas9 experiments were constructed from an uncoated 24x60 mm coverslip (Menzel-Gläser No. 1), double-sided adhesive tape (3M 467MP, 50 µm depth) and polyester film (Melinex 401, DuPont, 50 µm depth). Anti-digoxigenin (Roche) and BSA were adsorbed directly to the glass by incubation for >3 hours at room temperature. Each DNA construct was bound at its biotin-modified end to excess streptavidin-coated magnetic beads (1 µm diameter, MyOne, Invitogen) and added into the fluidic cell to allow the DNA to bind the surface via its digoxigenin-modified end. Non-magnetic particles (3.2 µm tosylactivated polystyrene or 2.0 µm aldehyde/sulphate latex, Invitrogen) were adhered to the glass (in phosphate buffered saline or 50 mM MES, pH 5.5, respectively) to correct for instrument drift. The three-dimensional position of the magnetic bead and thus the orientation and length of the attached DNA molecule was determined from video images at the camera frame rate (see above) using real-time 3D particle tracking with sub-nm accuracy (7-9). Suitable topologically-constrained DNA were identified from rotations curves and the rotational zero reference set as determined from a rotation curve at 0.3 pN. Experiments with Cascade were carried out in 20 mM Tris-HCl pH 8.0, 150 mM NaCl, 0.1 mg ml^{-1} BSA. Experiments with Cas9 were carried out in Buffer SB (see above). Measurements were performed using 9 nM Cascade (at room temperature), or using 1 nM Cas9 (at 25°C), unless otherwise noted. When recording the shift in rotational zero due to R-loop formation (see main text for details) magnets were rotated at 0.5 – 1.0 Hz. For measuring the on/off times as a function of torque, the magnets were turned at 1 Hz (Cascade) or 10 Hz (Cas9). In all time trajectories and rotation curves depicted, raw DNA length data taken at the camera acquisition rate is shown in light colours (light grey, blue or red), while data smoothed with either a 1 or 2 Hz moving average is shown as in dark colours (dark, blue, green, grey and red).

Determination of rotational shifts upon R-loop binding

At the typically applied concentration of Cascade of 9 nM, rotational shifts due to the formation of stable R-loops could only be determined from the shift of the right (positive) side of the rotation curve. This is due to the practically instantaneous R-loop formation at low negative twist, such that an “R-loop free” left side of the rotation curve could not be obtained (in contrast to Cas9, see below). Also, comparing the left side of a rotation curve with an R-loop to the left side of a rotation curve taken in absence of Cascade is not a reliable measure of the shift due to the observed DNA destabilization by Cascade which causes a shift in the left side even in the absence of an R-loop (see Fig. S9). For R-loop formation, the shift of the right side of the rotation curve is determined by fitting a straight line to the linear part of the rotation curve at positive turns before and after R-loop induction and determining the rotational shift of the midpoint of the fit ($-N_{loop}$ in Fig. 1*D*). For R-loop dissociation, the rotational shift is determined from the magnitude of the sudden DNA length increase upon R-loop dissociation. The length increase divided by the slope of the rotation curve at the corresponding force provides then the rotational shift ($+N_{loop}$ in Fig. 1*D*). The rotational shifts both upon R-loop formation and

dissociation are in agreement within error (Fig. 1*E*). In addition, the dissociation data also provides the rotational shift of the substep.
Using the shift of the right side of the rotation curve only assumes that the curves in the absence and presence of an R-loop exhibit an identical shape. To test this assumption, but also to obtain a method to extract rotational shifts for the DNA substrates with unstable R-loops, we carried out experiments at decreased Cascade concentrations (Fig. S3*A*). Under such conditions, R-loop formation becomes limited by Cascade binding and full rotation curves with and without R-loop formation events can be obtained in one experiment. Curves with and without R-loops were grouped and for each type an average rotation curve was obtained (Fig. S3*B*). The rotational shift of the curve centre is determined by fitting the peak of each average curve with a parabolic function and calculating the shift of the maximum position of the fit. The curve in the presence of an R-loop appears to be slightly broader and has a slightly lower maximum then the curve in absence of the R-loop. Thus, the shift of the right side of the rotation curve underestimates the shift of the curve centre, while the shift of the left side of the rotation curve overestimates the shift of the curve centre (Fig. S3*B*). Rotational shifts given in the case of stable R-loops were determined from the shift of the rotation curve centre at low Cascade concentrations, unless otherwise noted. In the case of unstable R-loops, rotational shifts were determined from the shift of the left side of the rotation curve at low Cascade concentrations, from which 0.15 turns were subtracted to correct for the curve broadening in the presence of the R-loop.

On the majority of Cas9 DNA substrates, R-loop formation and dissociation events occurred in the postbuckling/constant torque regime (see Fig. 1*F*). The position of the rotational zero could therefore be estimated before and after R-loop formation by fitting the peak of the induction and probe rotation curves to a parabolic function, as above.

Cas9 DNA cleavage assay in bulk

Cas9 DNA cleavage reactions were initiated by mixing supercoiled plasmid DNA with pre-assembled Cas9-crRNA-tracrRNA complex (1:1 v/v ratio) and performed at 25°C. Final reaction mixture contained 3 nM plasmid, 50 nM Cas9, 10 mM Tris-HCl (pH 7.5 at 37°C), 100 mM NaCl, 1 mM DTT and 10 mM $MgCl_2$ in a 100 µl reaction volume. Aliquots were removed at timed intervals and quenched with phenol/chloroform. The aqueous phase was mixed with 3× loading dye solution (0.01% (w/v) bromophenol blue and 75 mM EDTA in 50% (v/v) glycerol) and reaction products analysed by electrophoresis through agarose gels and ethidium bromide staining. The amount of supercoiled (SC), open circle (OC), and linear (FLL) DNA forms was evaluated by densitometric analysis of ethidium bromide stained gels using the software ImageJ. Values of reaction rate constants (see Fig. S6), were obtained as described earlier (10).

Cascade binding and Cas3-triggered DNA cleavage assays in bulk

Cascade binding experiments in bulk were carried out as described previously (3). In brief, increasing concentrations of Cascade were incubated with 0.1 nM radioactively labelled oligoduplex (Table S2) in binding buffer (40 mM Tris, 20 mM acetic acid, 1 mM ethylenediaminetetraacetic acid (EDTA), pH 8.0, 150 mM NaCl, 0.1 mg/ml BSA, 10% (v/v) glycerol) for 20 min at 37°C. Cascade-DNA complexes were analysed by 8% (w/v) polyacrylamide gels and visualized using a FLA-5100 phosphorimager (Fujilm). The dissociation constants (K_D values) for Cascade-DNA complexes were calculated as previously described (11). K_D values represent the average value of three independent experiments.
Cas3-triggered DNA cleavage was monitored as described previously (3). In brief, cleavage reactions were performed at 37°C for 10 min in nuclease buffer (10 mM Tris–HCl, pH 7.5, 75 mM NaCl, 40 mM KCl, 7% (v/v) glycerol, 1.5 mM $MgCl_2$, 0.1 mM $NiCl_2$, 2 mM ATP). Supercoiled plasmid DNA substrates (Table S2) at 5 nM concentration were incubated with 20 nM of

Cascade complex and 100 nM of Cas3. Reactions were initiated by addition of Cas3 and stopped by mixing with 3 × stop solution (67.5 mM EDTA, 27% (v/v) glycerol, 0.3% (w/v) SDS). Reaction products were analysed by electrophoresis using 0.8% (w/v) agarose gels and visualized by ethidium bromide staining.

SI theory – Torsional dependency of R-loop formation and dissociation rates

Torque during supercoiling DNA under tension

The behaviour of supercoiled DNA under tension, in particular the twist induced buckling and the subsequent plectonemic phase (see below) has recently attracted considerable interest (1,12-24). A summary of this behaviour according to previous work is given in the following.

When twisting torsionally relaxed DNA (denoted with 0 turns), the DNA length stays initially constant, while the torque increases linearly with turns (Fig. S1*B*):

$$\Gamma = \frac{C_S}{L} 2\pi N\,, \qquad \text{(S1)}$$

where Γ denotes the torque, L the DNA contour length, N the added number of turns and C_S the effective torsional modulus of DNA. The latter quantity is force dependent, since DNA fluctuations can absorb part of the twist (25,26):

$$C_S = C\left[1 - \frac{C}{4p \times k_B T}\left(\frac{k_B T}{p \times F}\right)^{1/2}\right], \qquad \text{(S2)}$$

with C being the nominal torsion modulus, F the stretching force and p the bending persistence length. We used C = 95 $k_B T$·nm (1,20,23,24,26) and p= 50 nm (27) throughout our analysis.

After a critical torque is reached (below torque values which would induce a structural transition within the B-form DNA structure), the DNA buckles, which is seen as a pronounced length jump that is accompanied by a torque "overshoot" (18,22,23). At this transition, a plectonemic superhelix is formed (for monovalent cation concentrations ≥20 mM). Upon further twisting, the DNA length then decreases linearly with the number of added turns, while the torque in the molecule remains roughly constant (Fig. S1*B*). This so-called "postbuckling" torque is, however, dependent on the applied force (increasing the force shifts the buckling point towards higher twist values) as well as on the concentration and type of cations in solution (19,20,28). To obtain a sufficiently precise estimate of the postbuckling torque, we use a previously developed theoretical model (19), that has been validated using experimental data (20) as well as Monte-Carlo simulations (19,24). To account for entropic effects (the confinement of the DNA within the plectonemic superhelix) that were not included in the theory, a force-independent torque offset of 1.5 pN nm is added to the torque obtained from the model, as revealed in Monte-Carlo simulations (19). A software tool with which the postbuckling parameters can be conveniently calculated is available for download at the author's website: http://www.uni-muenster.de/Biologie.AllgmZoo/Gruppen/Seidel/Download.

At sufficiently high torque the DNA helix undergoes structural transitions. Depending on the applied ionic conditions, for negative torque exceeding about 10 pN nm (about 0.8 pN stretching force in the plectonemic phase), the DNA helix either unwinds or adopts a Z-form-like left-handed DNA configuration (22,29). This is seen as the disappearance of the plectonemic phase for negative turns, such that the DNA supercoiling curve becomes asymmetric (see Fig. S7). Similarly, a structural transition occurs also for positive torque exceeding 30-40 pN nm (about 5 pN stretching force), where an overwound DNA structure is formed (so-called P-DNA) (30).

Torque dependence of R-loop formation and dissociation rates

To model the torque dependence of R-loop formation and dissociation, we assume that these processes are first-order/pseudo first-order reactions, which are governed by a single reaction

rate. This assumption is supported by the exponential distribution of the individual reaction times (Fig. S4).

The R-loop formation and dissociation rates k_{in} and k_{out}, are related to the free energy difference to reach the respective activation barrier ($\Delta G^*_{in/out}$) of the reaction according to the Arrhenius equation with frequency factor A:

$$k_{\text{in/out}} = A\,\mathrm{e}^{-\Delta G^*_{\text{in/out}}/k_\mathrm{B}T}. \tag{S3}$$

If during the reaction mechanical work W^* is carried out, e.g. due to a length change along an external force or as in our case due to a twist change in the presence of an external torque, the height of the barrier is changed by the performed work (31) resulting in:

$$\begin{aligned} k_{\text{in/out}}\left(W^*\right) &= A\,\mathrm{e}^{-\left(\Delta G^*_{\text{in/out}} - W^*_{\text{in/out}}\right)/k_\mathrm{B}T} \\ &= k_{\text{in/out}}\left(W^*=0\right)\mathrm{e}^{W^*_{\text{in/out}}/k_\mathrm{B}T}. \end{aligned} \tag{S4}$$

In order to derive a relationship for the torque dependent rates within this simple model, we have therefore to derive expressions for the mechanical work during our reaction. For quantifying R-loop association and dissociation of Cas9 as well as R-loop dissociation of Cascade, we ensured that for both the associated and the dissociated state the DNA was still in the plectonemic state (Figs. 2*A,D*). In these cases we can therefore consider the torque to be constant during the transition. Thus, the work done until the transition state $W^*_{in/out} = -\Gamma_{in/out}\, 2\pi\, \Delta N^*_{in/out}$, with $\Delta N^*_{in/out}$ being the distances of the respective initial state to the transition state (see Fig. S1*C*). This results in:

$$k_{\text{in/out}}\left(\Gamma\right) = k_{\text{in/out}}\left(\Gamma=0\right)\mathrm{e}^{-\Gamma_{\text{in/out}}\,2\pi\Delta N^*_{\text{in/out}}/k_\mathrm{B}T} \qquad \text{for constant } \Gamma_{\text{in/out}}. \tag{S5}$$

R-loop formation for Cascade occurred however in the non-plectonemic, i.e. linearly extended DNA state (see Figs. 2*A,B*, main text; due to the linearity the both torque and turn axes are given). Thus, the torque during this transition is linearly increasing with the induced DNA twist according to Eqn. S2. The work done until the transition state (see Fig. S1*C*) is then provided by:

$$\begin{aligned} \Delta W^*_{\text{in/out}} &= -\int_{N_{\text{in/out}}}^{N_{\text{in/out}}+\Delta N^*_{\text{in/out}}} \Gamma\cdot 2\pi\Delta N = -\frac{C_s}{L}(2\pi)^2 \int_{N_{\text{in/out}}}^{N_{\text{in/out}}+\Delta N^*_{\text{in/out}}} N\cdot dN \\ &= -\frac{C_s}{L}(2\pi)^2\,\frac{1}{2}\left(\left(N_{\text{in/out}}+\Delta N^*_{\text{in/out}}\right)^2 - \left(N_{\text{in/out}}\right)^2\right) \\ &= -\frac{C_s}{L}(2\pi)^2\,\Delta N_{\text{in/out}}\left(N_{\text{in/out}}+\frac{\Delta N^*_{\text{in/out}}}{2}\right) \end{aligned} \tag{S6}$$

where $N_{in/out}$ is the number of turns added for the initial state before the transition. Inserting this equation into Eqn. S4 provides then for torque dependence of the rates in case of a linearly changing torque:

$$k_{\text{in/out}}\left(N\right) = k_{\text{in/out}}\left(W^*=0\right)\mathrm{e}^{-\frac{C_s}{L}(2\pi)^2\,\Delta N^*_{\text{in/out}}\left(N_{\text{in/out}}+\frac{\Delta N^*_{\text{in/out}}}{2}\right)\Big/k_\mathrm{B}T} \qquad \text{for } \Gamma_{\text{in/out}} = \text{linear}. \tag{S7}$$

Note that for this equation zero work is not equivalent to zero turns or torsion, since the work is integrated from the initial state $N^*_{in/out}$ to the end state. The relations for the mean R-loop formation and dissociation times are obtained by taking the reciprocal of Eqns. S5 and S7:

$$T_{\text{in/out}}\left(\Gamma\right) = T_{\text{in/out}}\left(\Gamma=0\right)\mathrm{e}^{\Gamma_{\text{in/out}}\,2\pi\Delta N^*_{\text{in/out}}/k_\mathrm{B}T} \qquad \text{for constant } \Gamma_{\text{in/out}} \tag{S8}$$

$$T_{\text{in/out}}(N) = T_{\text{in/out}}(W^* = 0)\mathrm{e}^{\frac{C_s}{L}(2\pi)^2 \Delta N^*_{\text{in/out}}\left(N_{\text{in/out}} + \frac{\Delta N^*_{\text{in/out}}}{2}\right)\Big/ k_B T} \qquad \text{for linear } \Gamma_{\text{in/out}} \qquad \text{(S9)}$$

Constructing an energy landscape for R-loop formation by Cascade

Fitting the torque dependent mean times for R-loop formation and dissociation (Figs. 2*B,E* main text) provides the distance to the transition state of the particular transition and the mean transition time in absence of mechanical work or torque, as occurring on linear DNA or nicked plasmid DNA (Table S1).

Protein	**Transition**	**Barrier distance** (turns)	**Transition time in absence of torsion** (s)
Cascade	formation 1*	1.5±0.2	850 ± 100
	formation 2*	1.5 ± 0.2	3,000 ± 300
	dissociation 1st step	-0.31 ± 0.05	$104{,}000^{+300{,}000}_{-77{,}000}$
	dissociation 2nd step	-0.15 ± 0.06	37 ± 56
Cas9	dissociation	-0.5 ± 0.1	130 ± 100

Table S1. Parameters obtained from fitting the torque dependent mean times for R-loop formation and dissociation. * indicates that fitting results were obtained for two different data sets as shown for the R-loop formation in Fig. 2*B*.

Ratio between the mean R-loop dissociation time and the formation time provides the equilibrium constant K_{Rloop} for R-loop formation, which is related to the free energy difference for this process according to:

$$K_{\text{Rloop}} = \frac{T_{\text{out}}(0)}{T_{in}(0)} = \mathrm{e}^{-\Delta G_{\text{Rloop}}/k_B T} \qquad \text{(S10)}$$

For Cascade we could obtain estimates of both transition times. Its R-loop dissociation is limited by the first dissociation step (Table S1). Errors for the dissociation times at zero torsional energy are rather large in general, since the R-loop transitions are torque driven and occur (far from equilibrium and highly hysteretic) at elevated torque levels. Similarly the formation times at zero torque exhibit significant errors, due to an absolute precision of the zero torque position of about 0.1-0.2 turns. We used the limits of the transition times (Table S1) in order to estimate the free energy difference according to Eqn. S10. For Cascade we obtain a free energy difference for the R-loop formation between -2.1 and -6.3 $k_B T$, which is a rather small quantity given that the average base pairing/stacking energy of a single GC is ~3.4 $k_B T$. Using the obtained distances to the transition states, the free energy difference for R-loop formation and the supercoiling differences during full and partial R-loop formation/dissociation we can derive a model for the energy landscape of R-loop formation by Cascade (Fig. 2*C*, distances between energetic minima denoted by double-headed arrows were derived from supercoiling changes). Here we assume that the formation follows the same path as the dissociation, i.e. that it also passes the intermediate level at similar position. The independently obtained distances are, within error, consistent. The high R-loop stability of

Cascade is not achieved through a large free energy gain, but rather due to a slow kinetics combined with a highly skewed energy landscape. The large transition state distance for R-loop formation makes this step highly torque sensitive. In contrast, the transition state for the first dissociation step is close to the stable R-loop ground state, which reduces the torque dependence of R-loop dissociation compared to R-loop formation. This together causes the torsional resistance of bound Cascade.

In contrast to Cascade, the Cas9-dependent R-loop association times were strongly dependent on protein concentration (Fig. 2*E*). Extending the concentrations above 8 nM led to extensive noise on the DNA which masked the R-loop transitions, compounded by the fact that the transitions also became very rapid. Therefore, we were not able to demonstrate any torque-dependence for the association events. The strong dependence of R-loop formation on the Cas9 concentration, with mean formation times <1 s at 8 nMCas9, suggests a significant involvement of three-dimensional diffusion during the search for PAM sequences and matching protospacers. In addition, this dependence suggests that PAM identification and binding is the limiting step for Cas9, in agreement with the observation that Cas9 spends more time on DNA with cognate PAMs (32). For Cascade, PAM binding appears not to be limiting and this suggests that, for this complex at least, torque dependent R-loop priming accompanied by DNA helix destabilization is the crucial step. Thus, Cascade could directly scan homologous base pairs in a PAM modulated manner rather than primarily searching for a particular PAM. This would also explain the rather short and degenerate Cascade PAM sequences.

Overall, R-loop formation and dissociation occurs more rapidly for Cas9 compared to Cascade. This, together with the larger barrier distance for dissociation (-0.5±0.1 turns), gives rise to the lower resistance against external torque. At the experimental time scale, R-loop formation-dissociation appears to be hysteretic, although it becomes an equilibrium process on the time scale of a few minutes (mean dissociation time at zero torque of ~130 s). Thus, Cas9 will be easily able to sample between matching and slightly mutated protospacers. Cas9 did not show a clear intermediate in the dissociation process. This most likely reflects the absence of an additional locking step as observed for Cascade. This additional lock due to a structural rearrangement of the protein also additionally increases the R-loop stability of Cascade relative to Cas9.

Reconciling the differences between Cascade and Cas9 during the R-loop formation with available structural data

Very recently, high resolution structures of the *S. pyogenes* Cas9 apo-complex (33) as well as the target DNA-bound Cas9 holo-complex with tracrRNA and crRNA (34) became available. The new structural data together with the electron microscopy structure of Cascade from *E. coli* (35) suggests explanations for the differences between *St*-Cascade and *St*-Cas9 observed here.

The most prominent difference between the two CRISPR-Cas systems is the presence of an additional locking step for Cascade (see above, discussion in main text and the bistability of R-loops for truncated protospacers in Fig. 4a,b). For Cascade, a large movement of the CasB dimer together with rotation of CasA and CasE is observed (35), representing a likely candidate for this locking step. We suggest that locking serves as an additional proof-reading to verify R-loop formation which is necessary for the considerably longer R-loop in Cascade. This signal may be required to trigger Cas3 recruitment and thus subsequent DNA cleavage.

The Cas9 data lacks evidence for a distinct locking step. In agreement with this, Cas9 only displays a major structural rearrangement (closure of the bi-lobed protein core) upon binding of tracrRNA (33). In contrast, DNA target strand-binding does not lead to structural

rearrangements of a similar magnitude (33,34). Thus, Cas9 must have other means to ensure a high fidelity of DNA degradation. One prominent observation in this respect is the all-or-none length threshold for R-loop formation (Fig. 4C). Cas9 appears to stringently prohibit R-loop formation on PAM proximal protospacer targets shorter than 13 bp. In contrary, targets ≥13 bp exhibit rapid and efficient R-loop formation over the whole complementary stretch. Additionally, while shortening the protospacer at the PAM distal end down to 13 bp reduced the R-loop stability somewhat (except for the hyperstable state for 13 bp), we did not observe a complete loss of stability as seen for Cascade with shortenings of a more modest 4 bp or more. The PAM proximal 12 bp of the Cas9 protospacer (aka the “seed” sequence) must play a special role in target discrimination, as well as R-loop stability, as suggested previously (36,37). In agreement with this, the atomic structure of the ternary complex shows that Cas9 amino acid residues establish many contacts with the DNA-RNA heteroduplex over the seed sequence, while far fewer contacts are seen for the downstream base pairs. Additionally the importance of the first 12 bp is supported by estimating the transition state distance for R-loop formation. Assuming a simple two state system, and using the full untwisting upon R-loop formation of 1.45 turns and the transition state distance for R-loop dissociation of 0.5 turns, we obtain a value of 0.95 turns, equivalent to about 13 bp. Nonetheless, Cas9 uses an additional proof-reading step for the PAM distal end, which is subsequent DNA cleavage. Cleavage activity is already reduced for a 1 bp end truncation and further diminishes as the truncation increases (see Fig. S6); this effect is much more pronounced than the small change in R-loop stability. Proofreading of the protospacer distal end to activate the cleavage most likely occurs through stacking and hydrophobic interactions at the 5´ crRNA end alongside further DNA/RNA backbone contacts (34).

SI figures

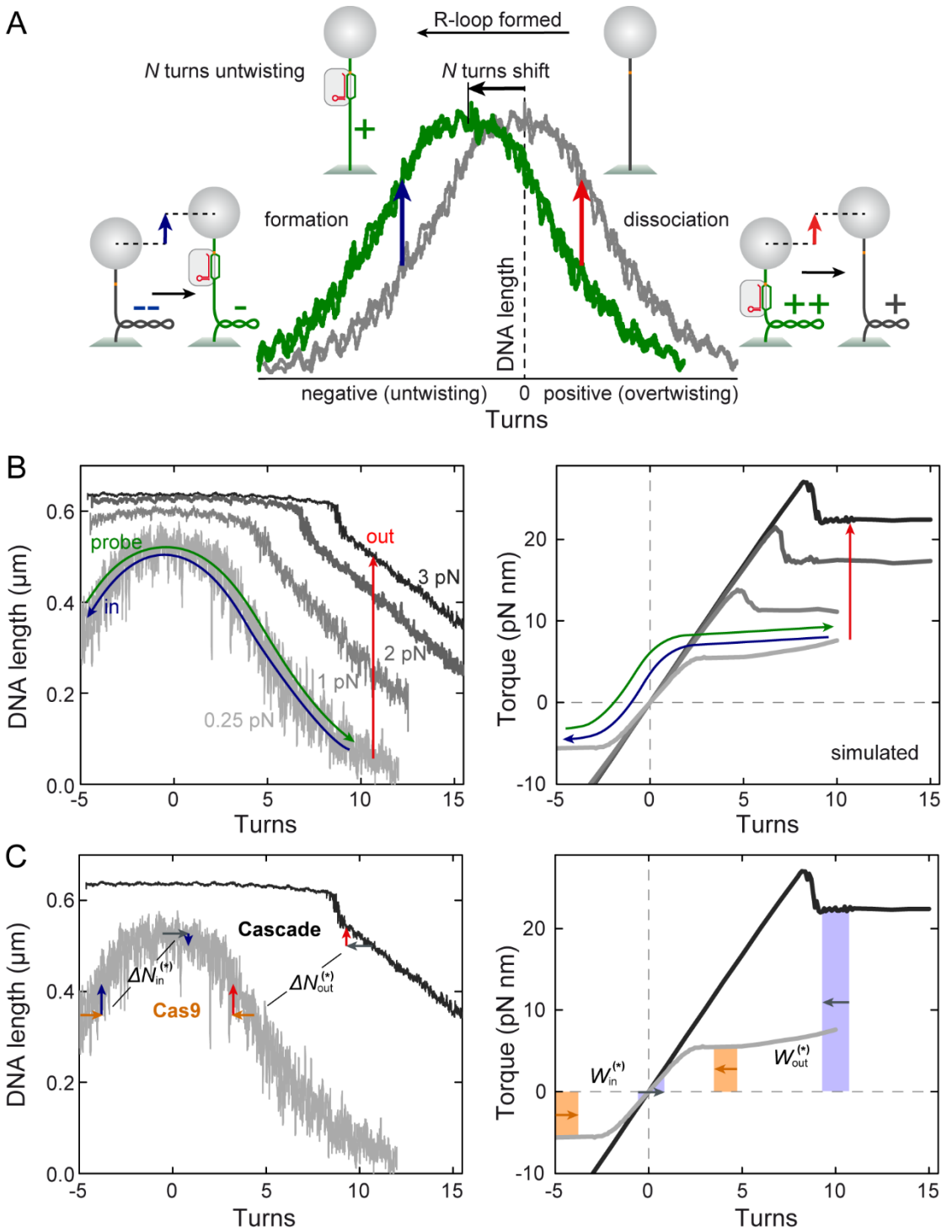

Fig. S1. Illustration of twist, DNA length, torque and work associated with supercoiling changes due to R-loop formation. (*A*) Twist and length changes upon R-loop formation and dissociation. The formed R-loop unwinds the DNA locally by *N* turns which leads to corresponding global overtwisting of the whole molecule (see sketches on top). This can be seen as a shift of the rotation curve without R-loop (gray curve) by –*N* turns (green curve). R-loop formation at a fixed number of turns is seen as a DNA length change when transiting from the gray to the green curve (blue arrow, sketches on the left). For negative supercoiled DNA R-loop formation leads to a length increase. Correspondingly R-loop dissociation at fixed turns corresponds to the DNA length change from the green to the gray curve (red arrow, sketches

on the right). For positive supercoiled DNA it leads also to a length increase. See also *C* for the specific length changes upon R-loop formation and dissociation for Cascade and Cas9. (*B*) DNA length (left) and torque (right, from Monte-Carlo simulations) during DNA supercoiling at different forces in the presence of 170 mM monovalent salt. Data was taken from Ref. (24). Illustrated are the changes in DNA length and torque during the R-loop cycle (Fig. 1) including R-loop induction (blue arrow), R-loop probing and a dedicated R-loop dissociation phase at high force/torque in case of Cascade (red arrow). (*C*) Illustration of changes in DNA length, torque and associated work *W* when measuring the torque dependence of R-loop formation and dissociation (Fig. 2). Blue and red arrows indicate DNA length changes during R-loop formation (in) and dissociation (out), respectively. Horizontal arrows indicate supercoiling changes during these processes (orange for Cas9, grey for Cascade). (Note that the arrows have opposite polarity to Fig. 1 since they do not indicate a shift of the rotation curve but rather a supercoiling change within the molecule.) Asterisks refer to the respective transition state. Orange and blue shaded areas in the torque plot indicate the work associated with a particular supercoiling state. While the measurements were done in the constant torque regime in all cases for Cas9 and for the R-loop dissociation cases for Cascade, R-loop formation for Cascade was measured in the linear torque regime.

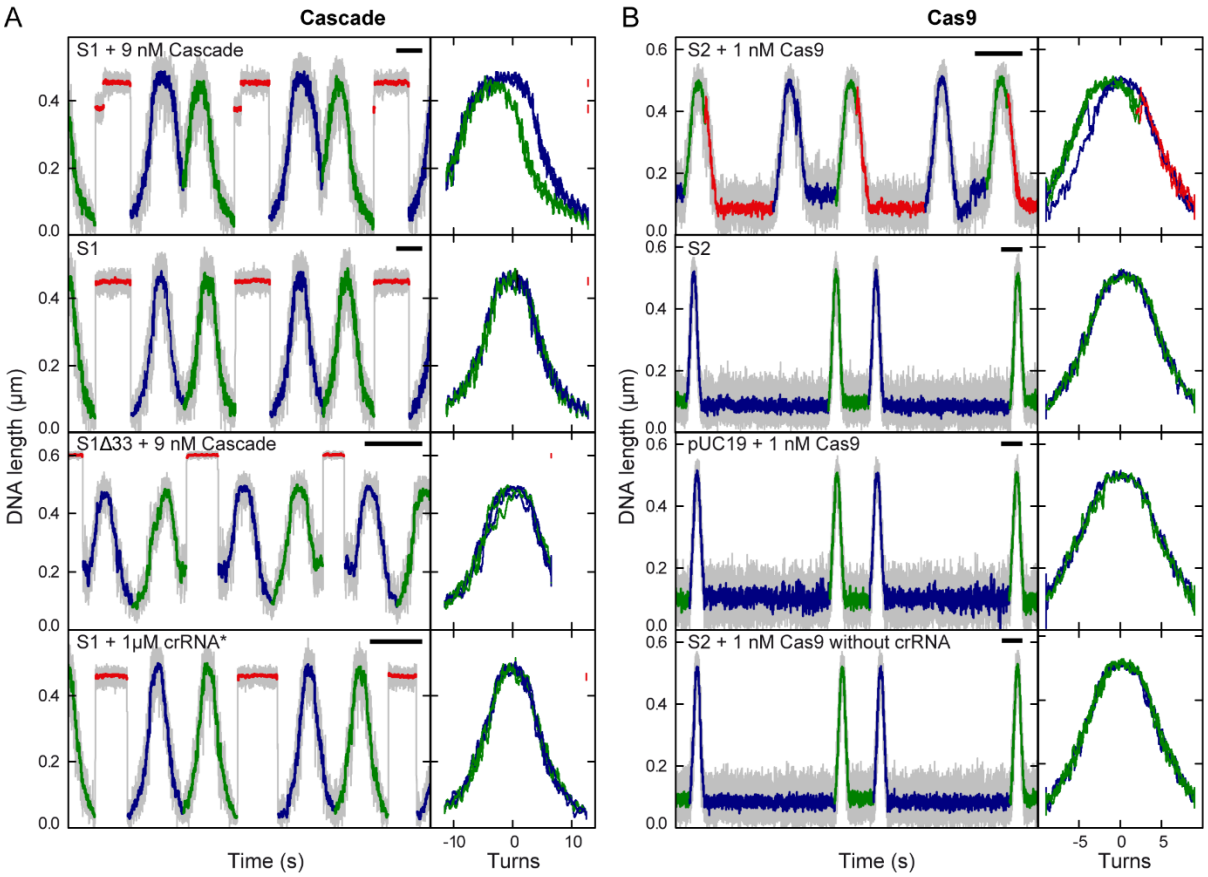

Fig. S2. Experimental controls for R-loop formation by Cascade and Cas9. (*A*) R-loop cycle experiments as in Figs. 1*C,D* for DNA constructs with an AA PAM and either a matching protospacer (S1, see Fig 1*A*) or a non-matching protospacer (S1Δ33, see Table S2) in the presence of 9 nM Cascade or 1 μM crRNA*. crRNA* is identical over the first 45 nts to the full-length crRNA (i.e. as in Fig. 1*A* but lacking the CasE-bound hairpin). R-loops were only observed for protospacer S1 in the presence of Cascade. Unlike the experiments with the CC-PAM DNA (Fig. 3*A*), R-loops did not form at extended negative supercoiling and waiting times, neither in the presence of the crRNA* alone on the S1 construct (1 h at -400 turns) nor in the presence of Cascade on the S1Δ33 construct (1 h at -200 turns). (*B*) R-loop cycle experiments as in Figs. 1*E*,*F* for a protospacer S2 construct (with a wild type protospacer-PAM) or a pUC19-derived construct (lacking a protospacer but with 77 orphan PAM sites) in the presence of 1 nM Cas9 + crRNA/tracrRNA or 1 nM Cas9 alone. R-loops were only observed with the S2 containing DNA and Cas9 + RNA. The time scale bar for all graphs is 50 s.

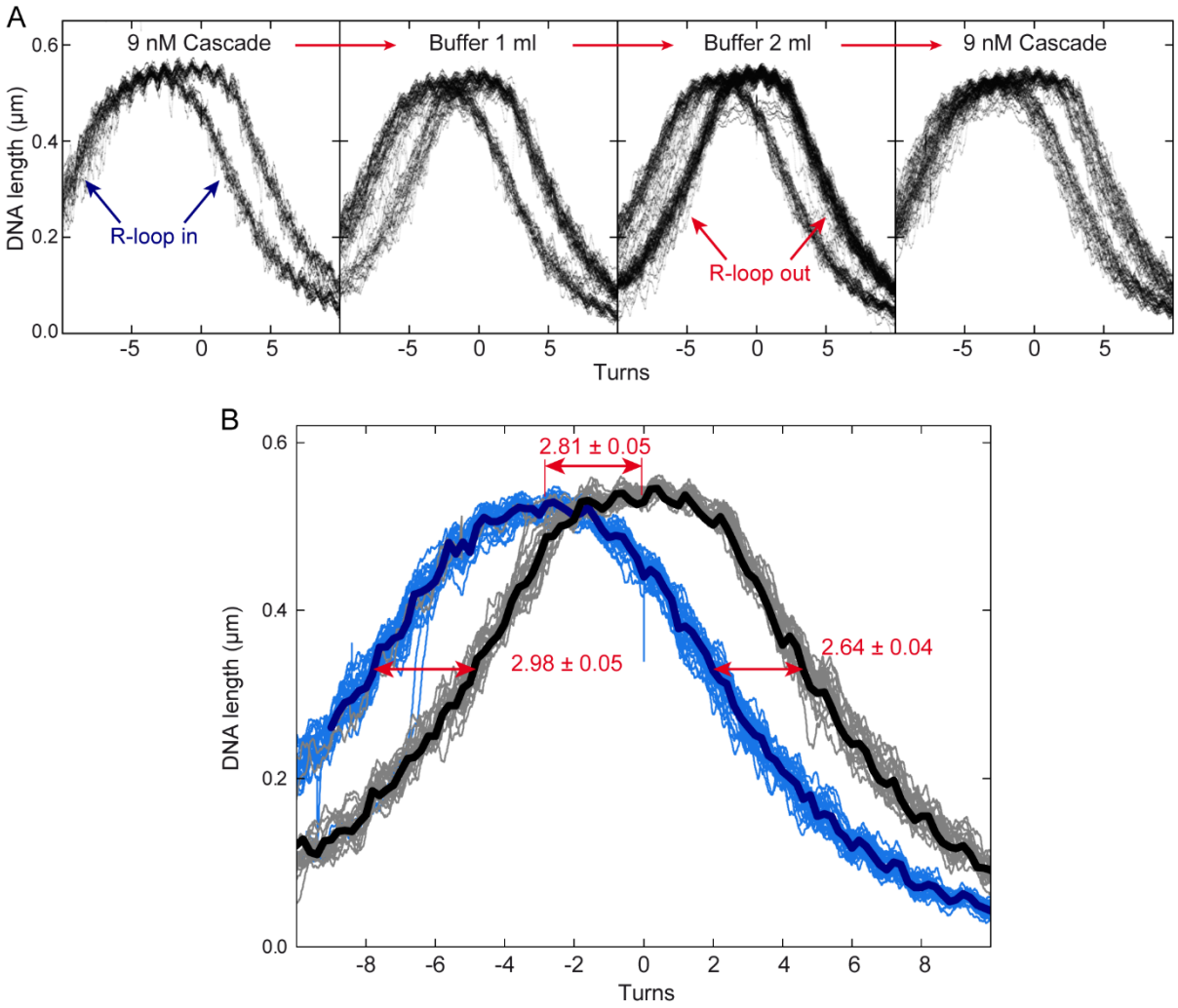

Fig. S3. R-loop cycles at low Cascade concentrations and determination of rotational shifts. (*A*) Successive R-loop cycle experiments for the DNA construct with matching protospacer and AA PAM in the presence of 9 nM Cascade, after flushing with 1 ml reaction buffer, after a second flush with 1 ml reaction buffer and after re-adding 9 nM Cascade (from left to right, data taken on the same molecule, each plot contains ~25 cycles, R-loop dissociation at high force is not shown). The volume of the fluidic cell is ~50 µl. Both R-loop induction and probe traces are shown. After the first buffer flush, an R-loop is not formed for a minor fraction of the cycles. After the second flush, R-loops are not formed for the majority of cycles. After re-adding Cascade, R-loops were formed in 100% of the cycles. (*B*) Probe traces from *A* shown in light blue if an R-loop was formed or in grey if an R-loop was not formed. The thick solid dark blue and black lines represent the averages of the two sets of traces. Red arrows indicate the shifts of the left side, the centre and the right side of the rotation curve when an R-loop was formed (see SI Materials & Methods). In the presence of an R-loop, the rotation curve is slightly broadened, as seen from the asymmetry of the shifts, and its maximum is slightly lowered. For DNA substrates with stable R-loops, the rotational shifts were determined from the centre shift of the curve. For substrates with unstable R-loops (protospacer truncations ≥6 bp), the rotational shifts were determined from the shift of the left side only, including a correction for the observed curve broadening.

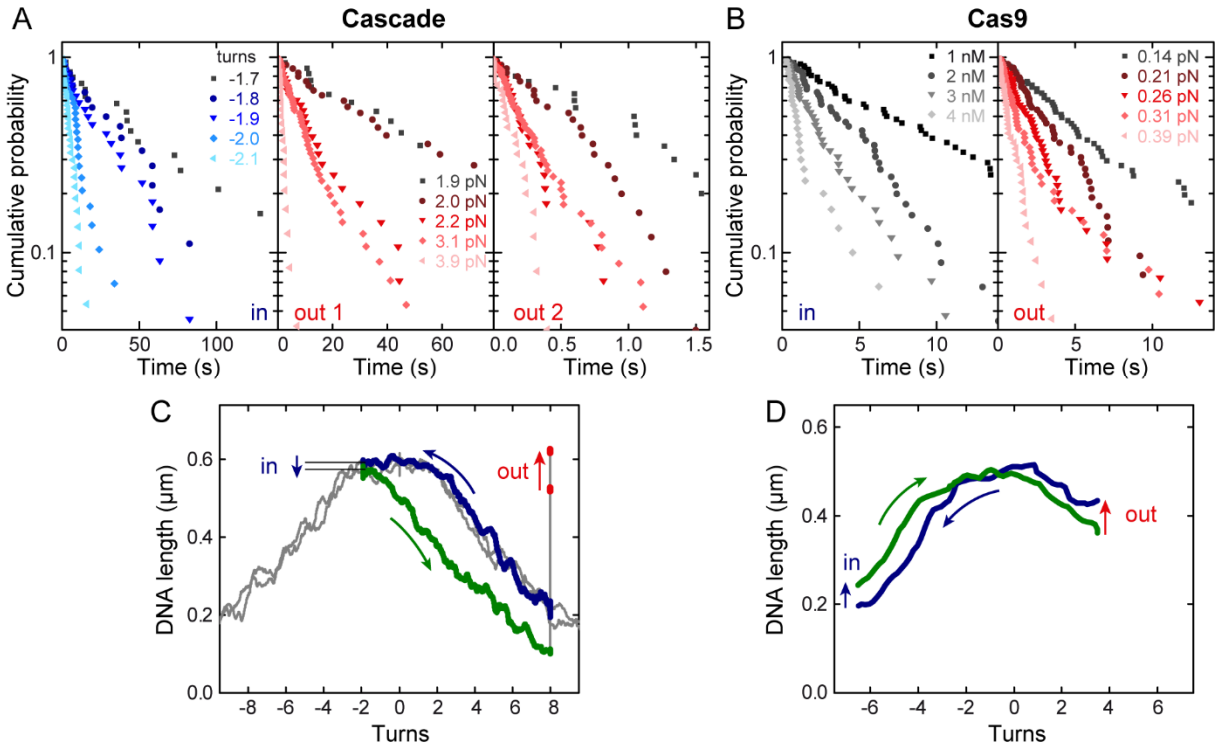

Fig. S4. Cumulative distributions of R-loop formation and dissociation times for different tensions. (*A*) Inverted cumulative distributions over time (probability that transition has not occurred) for R-loop formation (left) and the 1st and 2nd step of R-loop dissociation (middle and right) by Cascade. Mean times shown in Fig. 2*B* were calculated from this data. Experimental conditions are as in Fig. 2*B*. (*B*) Inverted cumulative probability over time for R-loop formation (left) and dissociation (right) by Cas9. Mean times shown in Fig. 2*E* were calculated from this data. Experimental conditions are as in Fig. 2*E*. (*C*) DNA length over turns at 1 Hz for one of the R-loop cycles in the presence of Cascade shown in Fig. 2*A* (green and blue curve, arrows indicate turning direction). The light grey curve was taken in absence of Cascade. R-loop formation can be observed as a slight length decrease at -2 turns (blue "in" arrow), while the R-loop dissociation occurred at higher forces and more extended DNA (red "out" arrow). (*D*) DNA length over turns at 10 Hz for one of the R-loop cycles in the presence of Cas9 that are shown in Fig. 2*D*. Blue ("in") and red ("out") arrows indicate the length jumps upon R-loop formation at fixed turn values.

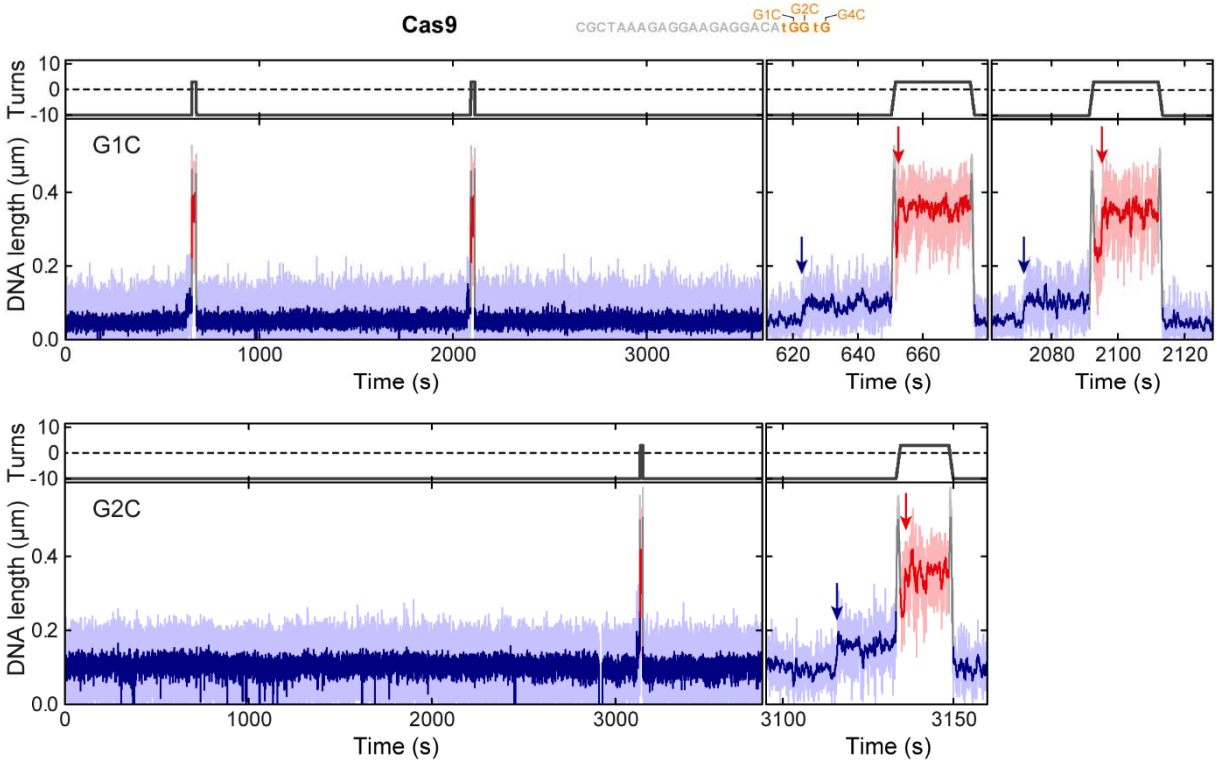

Fig. S5. PAM mutations that severely impede R-loop formation by Cas9. Extended time courses on DNA with protospacer S2 and PAM mutations G1C (*upper*) or G2C (*lower*) in the presence of 2 nM Cas9 and at F = 0.31 pN. DNA was rotated to -10 turns (blue stretches) to promote R-loop formation. Occasional reversible association of the bead with the surface can be observed. On the rare occasions that an R-loop formed, R-loop dissociation was promoted by rotation to +3 turns (red stretches). The right-hand panels show zoom-ins of the rare events. The observed R-loop out times have values within the expected range seen for wild type and G4C DNA (Fig. 3*D*). In contrast, the on times are slower than the G4C DNA and we could not observe sufficient numbers of events on a reasonable experimental time scale to obtain statistically-significant average time constants. Over similar time scales, events were never observed using a DNA where all three bases of the PAM were mutated (G1A, G2A, G4T). For all DNA tested with Cas9, R-loop formation could not be promoted using extended negative supercoiling as seen for Cascade (i.e. Fig. 3*A*).

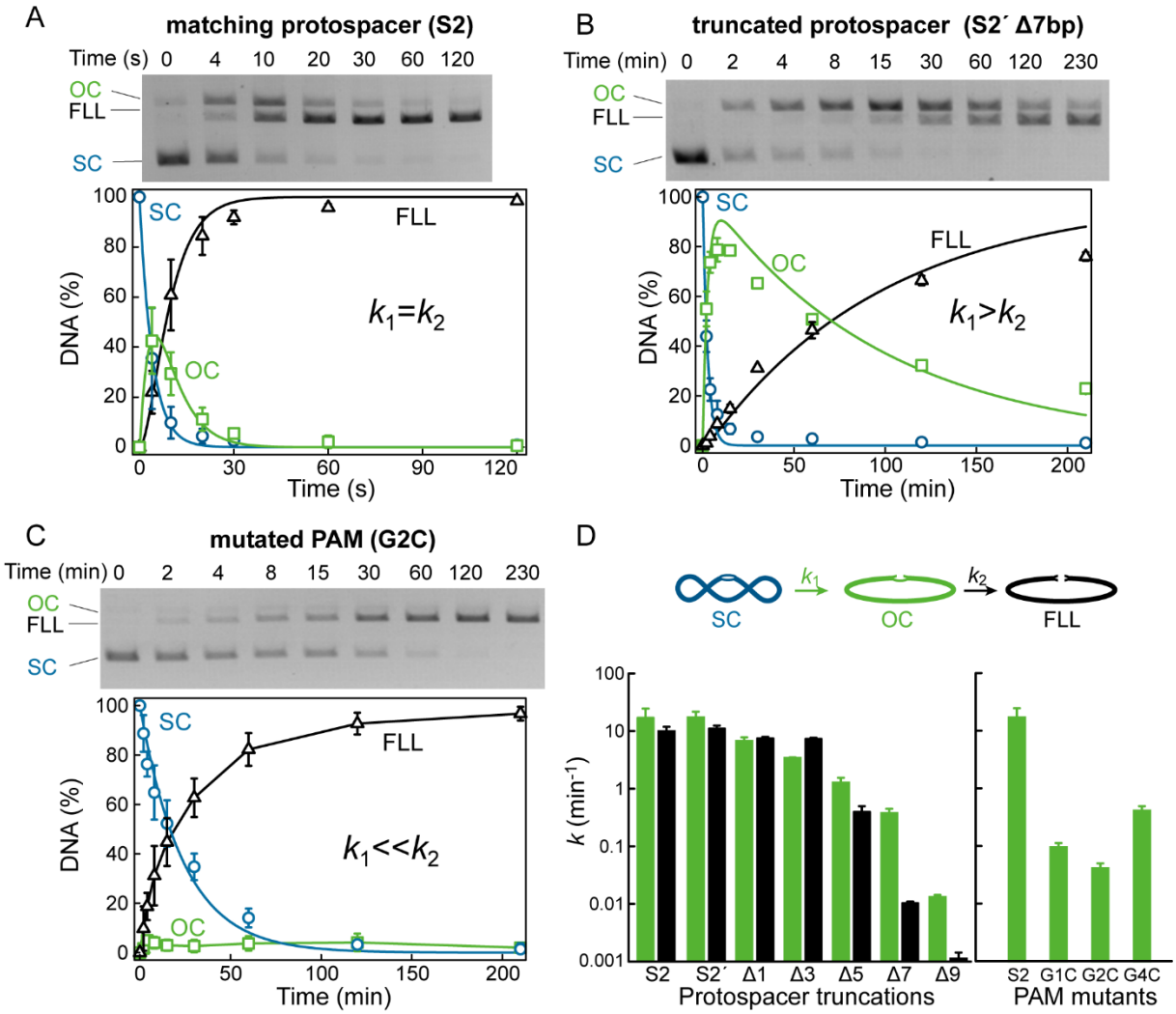

Fig. S6. Cleavage of plasmid DNA with end-truncated protospacers or mutated PAMs by the Cas9-crRNA-tracrRNA complex. (*A*) Plasmid containing a consensus GGNG PAM and a matching protospacer S2. Reaction products and intermediates were analysed by agarose gel electrophoresis (gel image shown on top) and quantified (shown below). SC (blue open circles) stands for a supercoiled substrate, OC (green open squares) stands for a nicked reaction intermediate cut at either DNA strand, and FLL (black open triangles) stands for a final reaction product cleaved at both DNA strands. Solid lines are fits to the data. (*B*) Cleavage reaction for a plasmid containing a consensus GGNG PAM and 7 bp protospacer truncation (S2′ Δ7 bp). (*C*) Cleavage reaction for a plasmid containing a G2C PAM mutation, and a matching protospacer S2. (*D*) Cleavage rates for the first and second DNA strand in plasmids containing protospacers with end truncations of different lengths but a consensus PAM (*left*) or a mutated PAM but a matching protospacer S2 (*right*). k_1 is the rate constant for formation of the nicked intermediate (including the first strand cleavage step and any preceding rate-limiting R-loop formation steps) whilst k_2 is the rate constant for the appearance of the final FLL product (including the second strand cleavage step) . k_1 and k_2 values were obtained by fitting the cleavage data as previously described (10). All data points are mean values from ≥3 independent experiments. Error bars are given as S.D. For the PAM mutants, the accumulation of nicked intermediate was not detected (see gel in panel c). Therefore only the k_1 value is provided. We can only estimate that $k_1<<k_2$ under these conditions. This is in agreement with a greatly reduced R-loop formation rate on these DNA. The actual cleavage rates of first and second strand after R-loop formation are expected to be as fast as for the consensus PAM - hence k_2 being much faster than k_1.

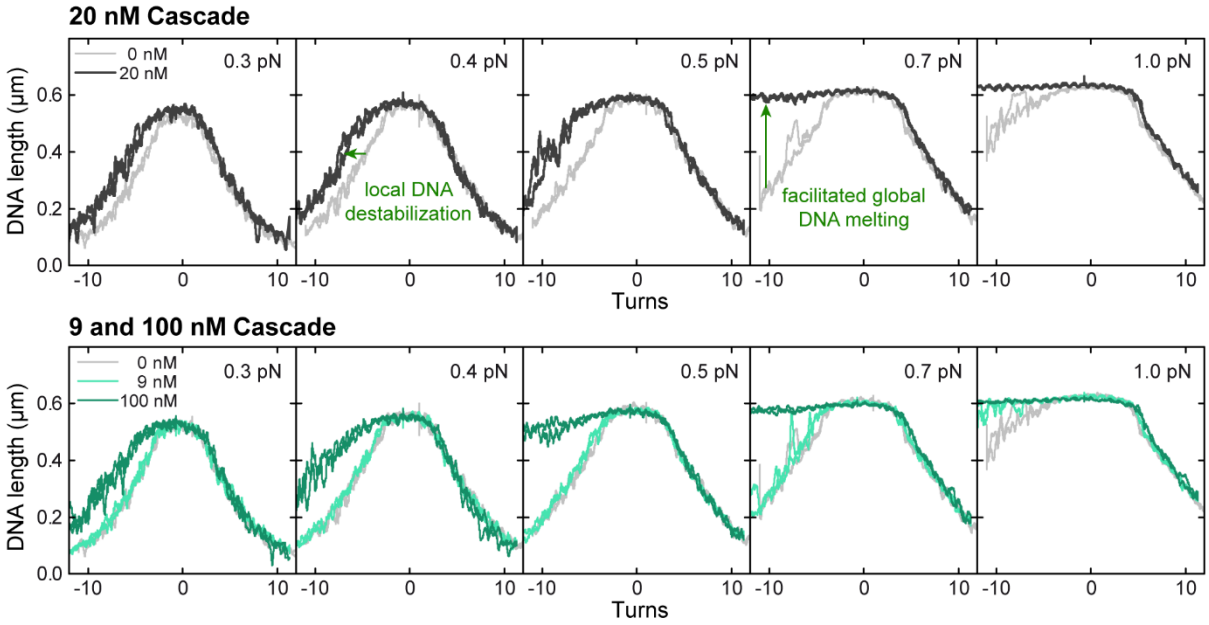

Fig. S7. DNA helix destabilization by Cascade. Supercoiling curves at different forces using DNA with a non-matching protospacer in the presence of different concentrations of Cascade. Rotation curves in the absence of Cascade are shown in light grey. In the absence of protein, the curves become asymmetric at forces above ~0.7 pN (12). The negative side of the supercoiling does not decrease as much as a function of turns as the positive side. At sufficiently high forces, the DNA length even remains about constant (see 1 pN data). This is due to melting of the B-form DNA structure and formation of denaturation bubbles or left-handed Z-form DNA, which releases the torsion in the DNA (1,21,22,29). In the presence of Cascade the negative side of the rotation curve is shifted to lower turns and the force for B-form DNA melting is lowered in a concentration dependent manner. Overall this behaviour is in agreement with a destabilization of the DNA structure due to Cascade. At low force/torque DNA melting is restricted to limited spots at which the DNA is sufficiently weakened leading only to a shift of the negative side of the rotation curve. At sufficient force/torque, the DNA appears to be weakened throughout its length, such that DNA melting occurs already between 0.5-0.7 pN for 20 nM Cascade and between 0.4-0.5 pN for 100 nM Cascade. For 9 nM Cascade destabilization effects are typically only seen at elevated forces (>0.7 pN). Note that the observed behaviour agrees only with DNA destabilization (i.e. lowering of the melting temperature) but not with active DNA helix distortion, as observed for DNA intercalators, where a shift of the full rotation curve towards negative turn values is observed (38,39). Insertion of aromatic amino acids residues of the CasA subunit into the DNA helix may be responsible for the observed helix destabilization as previously hypothesized (40) but this insertion will be a rather transient state rather than a stable bound state.

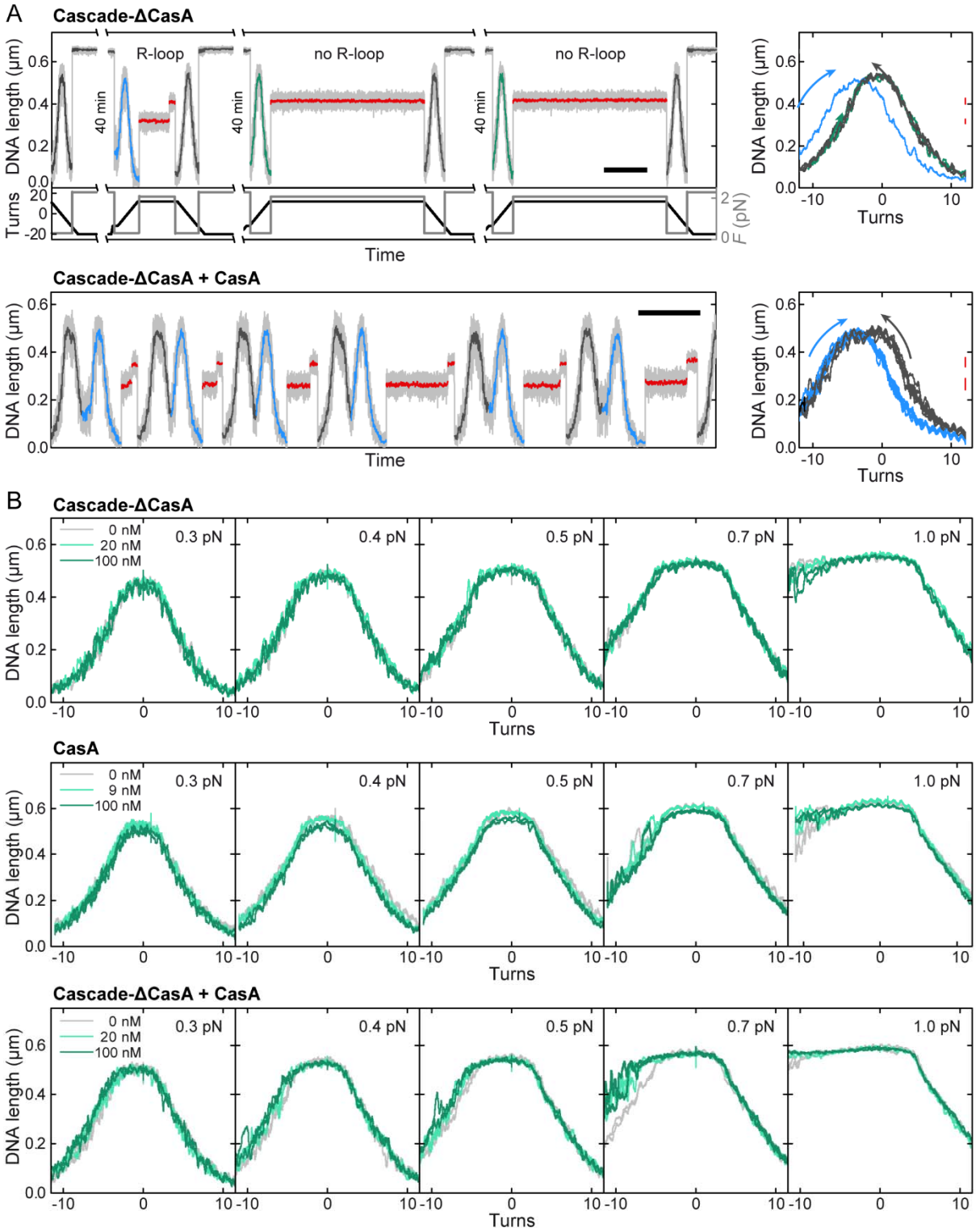

Fig. S8. Characterization of Cascade lacking the CasA subunit. To further investigate the DNA helix destabilization by Cascade (Fig. S7), we carried out twisting experiments with Cascade lacking the CasA subunit (Cascade-ΔCasA), CasA alone and the reconstituted complex from Cascade-ΔCasA mixed with CasA. (*A*) R-loop cycle experiments using DNA with matching protospacer in the presence of 9 nM Cascade-ΔCasA (*upper*) and 9 nM Cascade-ΔCasA + 9 nM CasA (*lower*). R-loop induction traces are shown in dark grey, probe traces with and without R-loops having been formed are shown in blue and green respectively, while dissociation traces are shown in red. Even Cascade-ΔCasA can form R-loops with 25% efficiency (N = 44) with high negative torsion (>2 pN force, -20 to -100 turns, no clear influence

of turn number observed) and elevated waiting times (40 min). Further quantification of R-loop formation was impeded due to the low efficiency and the long duration of this process. When adding Cascade-ΔCasA mixed with an equal amount of CasA, efficient R-loop formation similar to wt protein was restored. This provides evidence for the integrity of the Cascade-ΔCasA and CasA complex. (*B*) Supercoiling curves at different forces using DNA with a non-matching protospacer in the presence of different concentrations of Cascade-ΔCasA, CasA and reconstituted Cascade-ΔCasA. For Cascade-ΔCasA and CasA alone, no curve broadening indicative of DNA helix destabilization was observed, even in the presence of 100 nM protein. The reconstituted complex exhibits increasing shifts of the negative side of the rotation curve with increasing force from 0.3 to 0.5 pN and a facilitated DNA denaturation at 0.7 pN. The helix destabilization is less pronounced for the reconstituted complex compared to wt Cascade. Nonetheless, the effect is clearly visible. This suggests that CasA plays an important role in helix destabilization. Nonetheless the remainder of the Cascade complex is also required for helix destabilization. Possibly, the latter ensures sufficient non-specific DNA-binding by the full complex. Testing mutants of aromatic CasA residues that were identified to be crucial for PAM recognition in *E. coli* Cascade (40) should further corroborate the suggested helix destabilization by CasA. For *St*-Cascade the equivalent residues have yet to be identified.

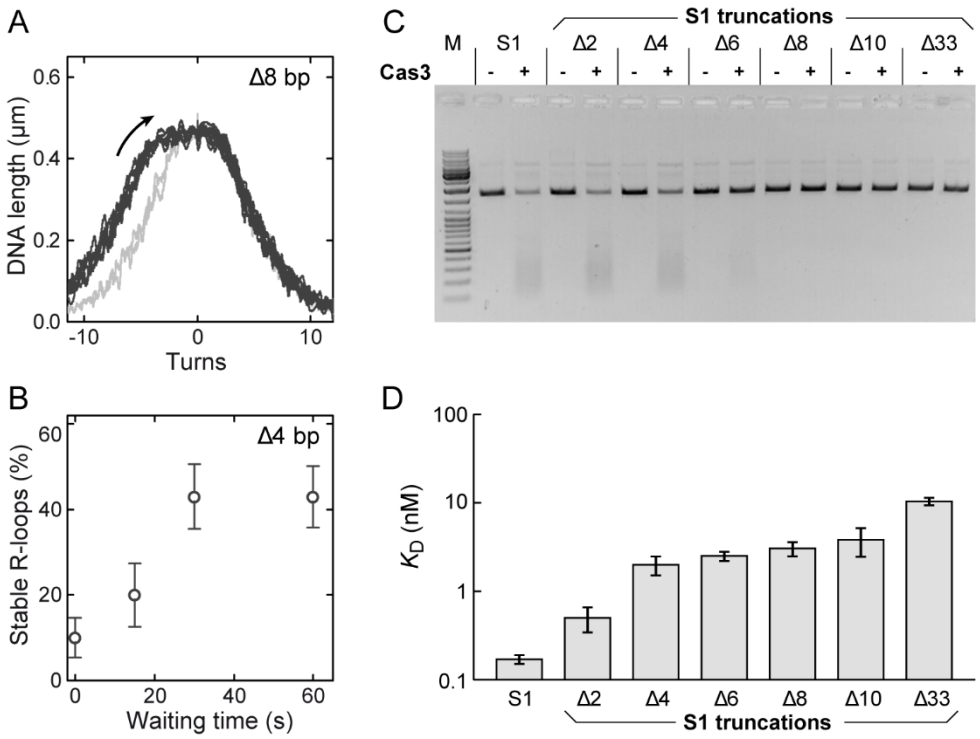

Fig. S9. R-loop formation by Cascade and Cas3-mediated DNA degradation on DNA with end-truncated protospacers (complementary to Figs. 4*A*,*B*). (*A*) R-loop probe curve in the presence of Cascade with a matching protospacer that was end-truncated by 8 bp (S1Δ8, see Fig. 4*A* for a sketch), revealing only unstable R-loops (dark grey). Light grey curves were taken in absence of Cascade. (*B*) Fraction of stable R-loops for the DNA with a protospacer end-truncated by 4 bp (S1Δ4, see Fig. 4*A*) as a function of waiting time at -12 turns and 0.3 pN force. A higher fraction of stable R-loops is achieved with increased waiting time, which suggests an additional locking step that increases the R-loop stability after initial R-loop formation. (*C*) DNA degradation assay in the presence of Cascade and Cas3 using different end-truncations of protospacer S1. S1 and S1Δ33 indicate, respectively, matching and non-matching protospacers for Cascade. Significant DNA degradation was only seen with the full-length protospacer and with the protospacers end-truncated by 2 or 4 bp. Stable R-loops were only detected in the single-molecule experiments using these substrates (Fig. 4*A*). Minor DNA degradation is observed for the protospacer end-truncated by 6 bp, whereas measurable DNA degradation was not detected for larger end-truncations. On these substrates only unstable R-loops were detected. (*D*) Dissociation constants of Cascade for different end truncations of protospacer S1. The dissociation constant increases with increasing truncation, though no direct relation to DNA degradation (see *C*) can be established. The dissociation constants (K_D values) for Cascade-DNA complexes were calculated as previously described (11). K_D values represent the average value of three independent experiments. Error bars are given as S.D.

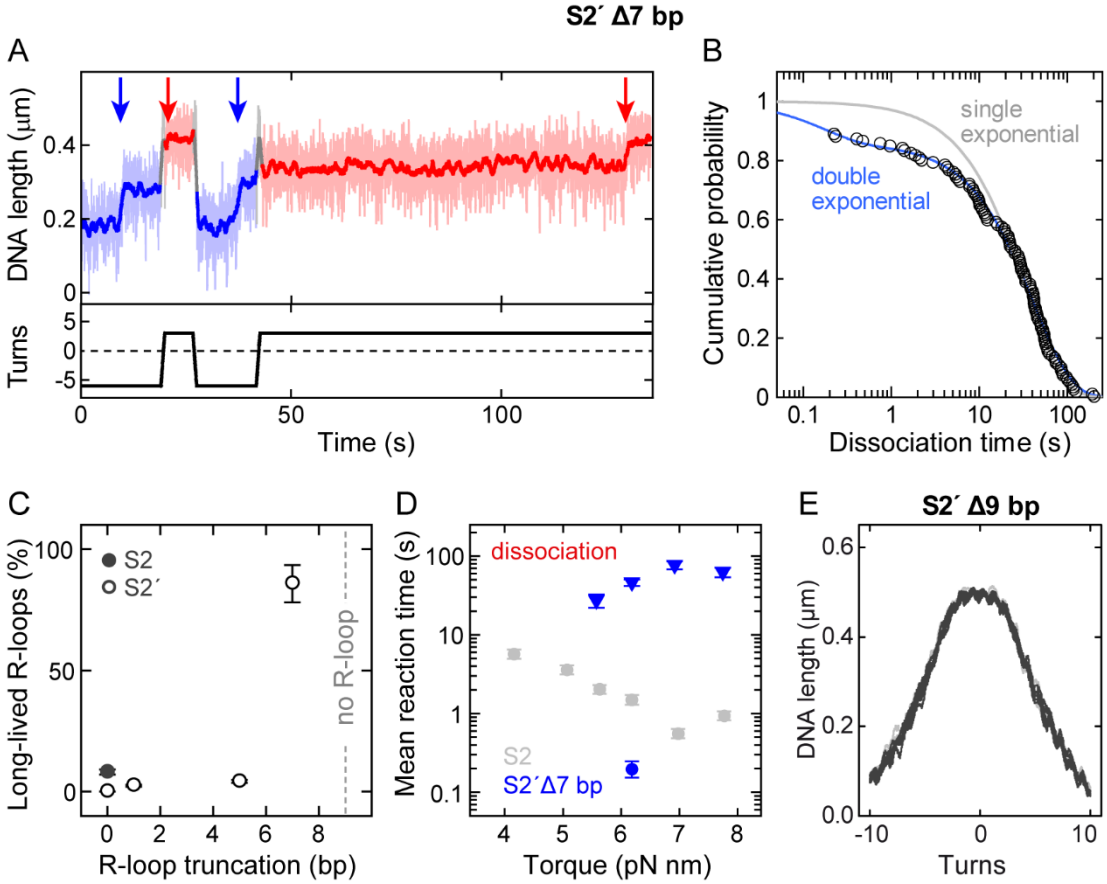

Fig. S10. Truncation of the Cas9 protospacer by 7 bp leads to formation of a long-lived, off pathway intermediate. (*A*) Time courses on DNA with protospacer S2′ truncated by 7 bp in the presence of Cas9. DNA was rotated to -6 turns (blue stretches) to promote R-loop formation. When an R-loop formed, R-loop dissociation was promoted by rotation to +3 turns (red stretches). The two dissociation events show a very fast reaction followed by a significantly slower reaction as indicated by the arrows. (*B*) Inverted cumulative probability over time for R-loop dissociation on S2′ Δ7 bp at a torque of 6.2 pN nm fitted to either a single or double exponential, as indicated. The better fit to the double exponential supports the presence of two populations (unstable vs long-lived). (*C*) The proportion of long-lived events seen on different DNA. This suggests a threshold over which the majority of R-loop events form off pathway intermediates before R-loop formation fails altogether. (*D*) R-loop dissociation times for S2′ Δ7 bp compared to S2 at different positive torque values. The fast events could not be accurately measured at torques above 6.7 pN nm because all the transition times were faster than the detection limit and the rate constant estimated from a double exponential fit became inaccurate. (*E*) R-loop probe curves in the presence of 1 nM Cas9 with S2′ Δ9 bp. The absence of a shift in the curves relative to the absence of Cas9 (light grey curves) indicates that R-loops of the expected length did not form.

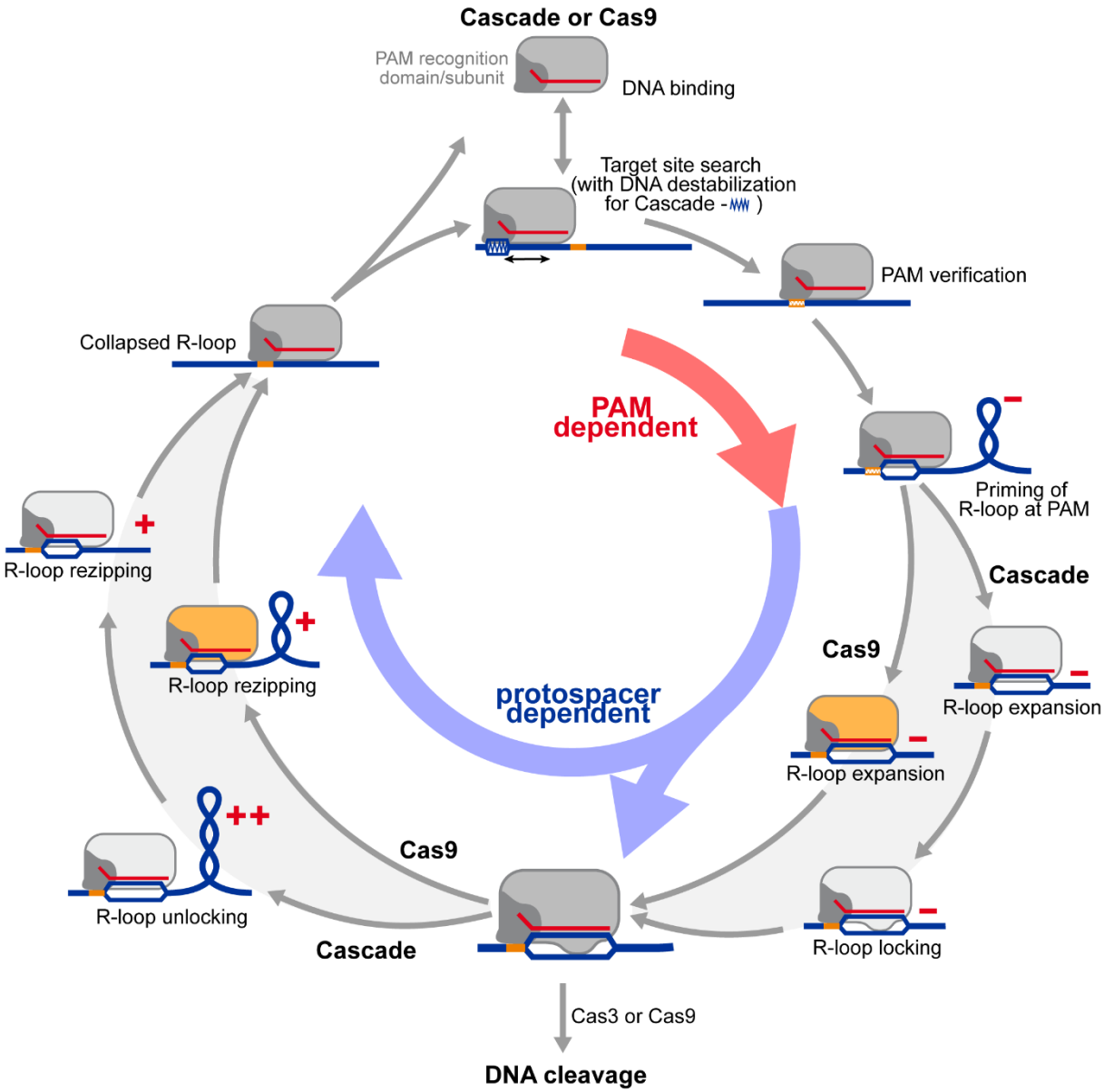

Fig. S11. Model for R-loop formation by Cascade and Cas9 involving the following steps**:** *(1) Target site search by the Cascade or Cas9 ribonucleoprotein (RNP) complex* - involving frequent, non-specific DNA association and dissociation events (see concentration dependencies in Figs. 2*E* and S3) and probably also 1D diffusion. Cascade employs DNA helix destabilization during this step (Figs. S7 and S8);

(2) *PAM recognition and verification* - occurring prior to R-loop formation by a specific domain or subunit of the RNP. The most likely PAM recognition domain of Cascade is CasA (40) (see Fig S8). The PAM controls the kinetics of R-loop formation (Fig. 3) most likely by ensuring the correct positioning of the complex with respect to the protospacer. PAM verification can be bypassed for Cascade by sufficient negative torque or prolonged waiting times, which can promote R-loop formation on a PAM that normally does not support fast DNA degradation (Fig. 4, Figs. S5 and S6) or by a complex lacking a PAM recognition subunit (Cascade-ΔCasA, Fig. S8);

(3) R-loop priming at PAM and further expansion - The R-loop becomes primed at the PAM, for example due to dsDNA destabilization or local denaturation (as shown for Cascade). In the presence of a matching protospacer, the R-loop rapidly expands downstream. In the case of Cas9 this occurs across the full length of the protospacer in a process governed by a single rate-limiting step;

(3b) R-loop locking (only for Cascade) - The R-loops becomes further stabilized by an additional conformational change during final R-loop expansion (as suggested by the two step dissociation) and most likely also involving rearrangements of the protein subunits of Cascade, e.g. the CasB dimer (35).This locking step gives rise to the extraordinary torsional stability of Cascade (see Figs. 2 and 4). For truncations of the protospacer end >4 bp, locking is no longer achieved;

(4) DNA cleavage – R-loops with full base pairing over the available crRNA length are efficiently cleaved by the intrinsic endonuclease activity of Cas9 or by the recruitment of the helicase-nuclease Cas3 by Cascade. For Cas9, R-loop shortening at the end opposite to the PAM progressively slows down the DNA cleavage rate and enriches nicked DNA intermediates. Even R-loops with a length of 11 bp exhibit such nicking, albeit being very slowly. This suggests that the correct positioning of the nuclease domains (which will determine the rate and concerted nature of cleavage) is conformationally-linked to the R-loop formation. For Cascade, DNA cleavage becomes almost completely inhibited by R-loop truncation as soon as the "locking" step fails, most likely due to the resulting increase in instable R-loops. This suggests that stable R-loops, and the accompanying conformational state(s) are necessary for Cas3 to be recruited. Overall, R-loop stability seems to play an important role for both CRISPR systems in determining entry to the DNA cleavage phase. i.e. not every R-loop event will lead to DNA cleavage, which is likely to be important in preventing cleavage of off-target sites. Once R-loops are formed, the PAM does not have a large influence on DNA cleavage, as suggested by the disappearance of the nicked intermediate for Cas9-based DNA cleavage (see Figs. 6*C*,*D*);

(5) *R-loop collapse before DNA cleavage* – R-loop formation is fully reversible. R-loops collapse occurs at low positive torque when a sufficient number of mismatches are present. Fully complementary R-loops are the most stable. Therefore, DNA torsion accumulated due to enzyme activity may be used *in vivo as* a regulator to discriminate complementary from mis-paired R-loops. Due to the "locking" step, the response of Cascade to mismatches is almost binary (i.e. either "on" or "off"). This may represent a proofreading step. We attribute the collapse of the "lock" to the first long-lived intermediate upon R-loop dissociation (see Fig. 2*A*), whereas the short-lived second step represents the final R-loop dissociation. This suggests a rather low torsional stability of R-loops in general.

In summary, R-loop priming is controlled by the PAM verification, whereas all downstream steps, such as R-loop expansion, R-loop locking, DNA cleavage and R-loop collapse are almost exclusively controlled by the base-pairing within the R-loop.

Table S2. Protospacer, PAM variants and PCR primers used in the Cascade experiments. Oligoduplexes shown below were inserted into the pUC19 vector pre-cleaved with SmaI. Engineered plasmids were used as substrates in the bulk cleavage experiments. PCR templates from these plasmids were used to prepare substrates for the magnetic tweezers experiments. The protospacer sequence complementary to the crRNA is underlined, PAMs are shown in red letters.

Name	Sequence	Description
S1	5′-GACCACCCTTTTTGATAT**AA**<u>**TATACCTATATCAATGGCCTCCCACGCATAAGC**</u>GCAGATACGTTCTGAGGGAA-3′ 3′-CTGGTGGGAAAAACTATA**TT**<u>**ATATGGATATAGTTACCGGAGGGTGCGTATTCG**</u>CGTCTATGCAAGACTCCCTT-5′	The 33 nt protospacer matching to the spacer-1 of the CRISPR4 system of *S. thermophilus*; PAM – AA;
S1Δ2	5′-GACCACCCTTTTTGATAT**AA**<u>**TATACCTATATCAATGGCCTCCCACGCATAA**</u>CGGCAGATACGTTCTGAGGGAA-3′ 3′-CTGGTGGGAAAAACTATA**TT**<u>**ATATGGATATAGTTACCGGAGGGTGCGTATT**</u>GCCGTCTATGCAAGACTCCCTT-5′	2 nt 3′-end truncation of the S1 protospacer; PAM – AA;
S1Δ4	5′-GACCACCCTTTTTGATAT**AA**<u>**TATACCTATATCAATGGCCTCCCACGCAT**</u>TTCGGCAGATACGTTCTGAGGGAA-3′ 3′-CTGGTGGGAAAAACTATA**TT**<u>**ATATGGATATAGTTACCGGAGGGTGCGTA**</u>AAGCCGTCTATGCAAGACTCCCTT-5′	4 nt 3′-end truncation of the S1 protospacer; PAM – AA;
S1Δ6	5′-GACCACCCTTTTTGATAT**AA**<u>**TATACCTATATCAATGGCCTCCCACGC**</u>TATTCGGCAGATACGTTCTGAGGGAA-3′ 3′-CTGGTGGGAAAAACTATA**TT**<u>**ATATGGATATAGTTACCGGAGGGTGCG**</u>ATAAGCCGTCTATGCAAGACTCCCTT-5′	6 nt 3′-end truncation of the S1 protospacer; PAM – AA;
S1Δ8	5′-GACCACCCTTTTTGATAT**AA**<u>**TATACCTATATCAATGGCCTCCCAC**</u>CGTATTCGGCAGATACGTTCTGAGGGAA-3′ 3′-CTGGTGGGAAAAACTATA**TT**<u>**ATATGGATATAGTTACCGGAGGGTG**</u>GCATAAGCCGTCTATGCAAGACTCCCTT-5′	8 nt 3′-end truncation of the S1 protospacer; PAM – AA;
S1Δ10	5′-GACCACCCTTTTTGATAT**AA**<u>**TATACCTATATCAATGGCCTCCC**</u>GCAGATACGTTCTGAGGGAA-3′ 3′-CTGGTGGGAAAAACTATA**TT**<u>**ATATGGATATAGTTACCGGAGGG**</u>CGTCTATGCAAGACTCCCTT-5′	10 nt 3′-end truncation of the S1 protospacer; PAM – AA;
S1Δ33	5′-GACCACCCTTTTTGATAT**AA**CGCAACCCCTCCTTAGACATGGGAACAGTACTAGCAGATACGTTCTGAGGGAA-3′ 3′-CTGGTGGGAAAAACTATA**TT**GCGTTGGGGAGGAATCTGTACCCTTGTCATGATCGTCTATGCAAGACTCCCTT-5′	No protospacer; PAM – AA.
S1-TT	5′-GACCACCCTTTTTGATAT**TT**<u>**TATACCTATATCAATGGCCTCCCACGCATAAGC**</u>GCAGATACGTTCTGAGGGAA-3′ 3′-CTGGTGGGAAAAACTATA**AA**<u>**ATATGGATATAGTTACCGGAGGGTGCGTATTCG**</u>CGTCTATGCAAGACTCCCTT-5′	PAM – TT; 33 nt S1 protospacer
S1-AG	5′-GACCACCCTTTTTGATAT**AG**<u>**TATACCTATATCAATGGCCTCCCACGCATAAGC**</u>GCAGATACGTTCTGAGGGAA-3′ 3′-CTGGTGGGAAAAACTATATC<u>**ATATGGATATAGTTACCGGAGGGTGCGTATTCG**</u>CGTCTATGCAAGACTCCCTT-5′	PAM – AG; 33 nt S1 protospacer
S1-GG	5′-GACCACCCTTTTTGATAT**CC**<u>**TATACCTATATCAATGGCCTCCCACGCATAAGC**</u>GCAGATACGTTCTGAGGGAA-3′ 3′-CTGGTGGGAAAAACTATA**GG**<u>**ATATGGATATAGTTACCGGAGGGTGCGTATTCG**</u>CGTCTATGCAAGACTCCCTT-5′	PAM – GG; 33 nt S1 protospacer

Table S3. Protospacer, PAM variants and PCR primers used in the Cas9 experiments. Oligoduplexes shown below were inserted into the pUC18 vector pre-cleaved with EcoRI. Engineered plasmids were used as substrates in the bulk cleavage experiments. PCR templates from these plasmids were used to prepare substrates for the magnetic tweezers experiments. The protospacer sequence complementary to the crRNA is underlined, PAMs are shown in red letters.

Name	Sequence	Description
S2	5'-AATTG**AAATTCTAAACGCTAAAGAGGAAGAGGACA**T**GG**T**G**-3' 3'-C**TTTAAGATTTGCGATTTCTCCTTCTCCTGT**A**CC**A**C**TTAA-5'	The 30 nt protospacer matching to the spacer-1 in the CRISPR3 system of *S. thermophilus*; PAM – tGGtG; crRNA in the Cas9 complex matches only 20 nt in the 30 nt protospacer
S2´	5'-AATTGTGACAG**CGCTAAAGAGGAAGAGGACA**T**GG**T**G**-3' 3'-CACTGTC**GCGATTTCTCCTTCTCCTGT**A**CC**A**C**TTAA-5'	A 20 nt protospacer matching to the 20 nt spacer of crRNA;
S2´Δ1	5'-AATTG**GCTAAAGAGGAAGAGGACA**T**GG**T**G**-3' 3'-C**CGATTTCTCCTTCTCCTGT**A**CC**A**C**TTAA-5'	1 nt 5′-end truncation of the S2´ protospacer (19 nt complementary to crRNA);
S2´Δ3	5'-AATTG**TAAAGAGGAAGAGGACA**T**GG**T**G**-3' 3'-C**ATTTCTCCTTCTCCTGT**A**CC**A**C**TTAA-5'	3 nt 5′-end truncation of the S2´ protospacer (17 nt complementary to crRNA);
S2´Δ5	5'-AATTG**AAGAGGAAGAGGACA**T**GG**T**G**-3' 3'-C**TTCTCCTTCTCCTGT**A**CC**A**C**TTAA-5'	5 nt 5′-end truncation of the S2´ protospacer (15 nt complementary to crRNA);
S2´Δ7	5'-AATTGCGATTT**GAGGAAGAGGACA**T**GG**T**G**-3' 3'-CGCTAAA**CTCCTTCTCCTGT**A**CC**A**C**TTAA-5'	7 nt 5′-end truncation of the S2´ protospacer (13 nt complementary to crRNA);
S2´Δ9	5'-AATTGCGATTTCT**GGAAGAGGACA**T**GG**T**G**-3' 3'-CGCTAAAGA**CCTTCTCCTGT**A**CC**A**C**TTAA-5'	9 nt 5′-end truncation of the S2´ protospacer (11 nt complementary to crRNA);
S2ΔPAM	5'-AATTG**AAATTCTAAACGCTAAAGAGGAAGAGGACA**-3' 3'-C**TTTAAGATTTGCGATTTCTCCTTCTCCTGT**TTAA-5'	no PAM; 30 nt S2 protospacer;
S2-G1C	5'-AATTG**AAATTCTAAACGCTAAAGAGGAAGAGGACA**T**CG**T**G**-3' 3'-C**TTTAAGATTTGCGATTTCTCCTTCTCCTGT**A**GC**A**C**TTAA-5'	G1C mutation in the PAM; 30 nt S2 protospacer;
S2-G2C	5'-AATTG**AAATTCTAAACGCTAAAGAGGAAGAGGACA**T**GC**T**G**-3' 3'-C**TTTAAGATTTGCGATTTCTCCTTCTCCTGT**A**CG**A**C**TTAA-5'	G1C mutation in PAM; 30 nt S2 protospacer;
S2-G4C	5'-AATTG**AAATTCTAAACGCTAAAGAGGAAGAGGACA**T**GG**T**C**-3' 3'-C**TTTAAGATTTGCGATTTCTCCTTCTCCTGT**A**CC**A**G**TTAA-5'	G4C mutation in PAM; 30 nt S2 protospacer;

Table S4. PCR Primers for tweezers construct preparation.

Template	Sequence	Description
pUC19-S1 and derivatives	5´-GCGTAAGTCTCGAGAACTAGTTCCGTAAGATGCTTTTCTGTGACT-3´ 5´-GCGTAAGTGCGGCCGCTTCGTTCCACTGAGCGTCAGA-3´	Primers for 2.1 kbp PCR fragment containing the protospacer S1 variants for the experiments with cascade.
pbluescriptSK+	5´-GACCGAGATAGGGTTGAGTG-3´ 5´-TTTGTGATGCTCGTCAGGGG-3´	1.2 kbp fragment for biotin and digoxigenin handles for ligation to the pUC19-S1 based PCR fragments
pUC18-S2 and derivatives	5´- GCGTAAGTCTCGAGAACTAGTTCCGTAAGATGCTTTTCTGTGACT-3´ 5´- GCGTAAGTGCGGCCGCTTCGTTCCACTGAGCGTCAGA-3´	Primers for 2.1 kbp PCR fragment containing the protospacer S2 variants for the experiments with Cas9.
pUC19	5´- GCGTAAGTCTCGAGAACTAGTAGAATAGTGTATGCGGCGACC-3´ 5´- GCGTAAGTGCGGCCGCTGACCATGATTACGCCAAGC-3´	1.0 kbp fragment for biotin and digoxigenin handles for ligation to the pUC18-S2 based PCR fragments

SI References

1. Kauert DJ, Kurth T, Liedl T, Seidel R (2011) Direct mechanical measurements reveal the material properties of three-dimensional DNA origami. *Nano Lett* 11(12):5558–5563.
2. Luzzietti N, Knappe S, Richter I, Seidel R (2012) Nicking enzyme-based internal labeling of DNA at multiple loci. *Nat Protoc* 7(4):643–653.
3. Sinkunas T, et al. (2013) In vitro reconstitution of Cascade-mediated CRISPR immunity in Streptococcus thermophilus. *EMBO J* 32(3):385–394.
4. Karvelis T, et al. (2013) crRNA and tracrRNA guide Cas9-mediated DNA interference in Streptococcus thermophilus. *RNA Biol* 10(5):841–851.
5. Seidel R, et al. (2005) Dynamics of initiation, termination and reinitiation of DNA translocation by the motor protein EcoR124I. *EMBO J* 24(23):4188–4197.
6. Revyakin A, Ebright RH, Strick TR (2005) Single-molecule DNA nanomanipulation: improved resolution through use of shorter DNA fragments. *Nat Methods* 2(2):127–138.
7. Klaue D, Seidel R (2009) Torsional stiffness of single superparamagnetic microspheres in an external magnetic field. *Phys Rev Lett* 102(2):028302.
8. Lionnet T, et al. (2012) Magnetic trap construction. *Cold Spring Harb Protoc* 2012(1):133–138.
9. Otto O, et al. (2010) Real-time particle tracking at 10,000 fps using optical fiber illumination. *Opt Express* 18(22):22722–22733.
10. Zaremba M, Sasnauskas G, Urbanke C, Siksnys V (2006) Allosteric communication network in the tetrameric restriction endonuclease Bse634I. *J Mol Biol* 363(4):800–812.
11. Tamulaitis G, Sasnauskas G, Mucke M, Siksnys V (2006) Simultaneous binding of three recognition sites is necessary for a concerted plasmid DNA cleavage by EcoRII restriction endonuclease. *J Mol Biol* 358(2):406–419.
12. Strick TR, Croquette V, Bensimon D (1998) Homologous pairing in stretched supercoiled DNA. *Proc Natl Acad Sci USA* 95(18):10579–10583.
13. Daniels BC, Forth S, Sheinin MY, Wang MD, Sethna JP (2009) Discontinuities at the DNA supercoiling transition. *Phys Rev E* 80(4 Pt 1):040901.
14. Neukirch S, Marko JF (2011) Analytical description of extension, torque, and supercoiling radius of a stretched twisted DNA. *Phys Rev Lett* 106(13):138104.
15. Emanuel M, Lanzani G, Schiessel H (2013) Multiplectoneme phase of double-stranded DNA under torsion. *Phys Rev E* 88(2):022706.
16. van Loenhout MTJ, de Grunt MV, Dekker C (2012) Dynamics of DNA supercoils. *Science* 338(6103):94–97.
17. Argudo D, Purohit PK (2012) The dependence of DNA supercoiling on solution electrostatics. *Acta Biomater* 8(6):2133–2143.
18. Brutzer H, Luzzietti N, Klaue D, Seidel R (2010) Energetics at the DNA supercoiling transition. *Biophys J* 98(7):1267–1276.
19. Maffeo C, et al. (2010) DNA-DNA interactions in tight supercoils are described by a small effective charge density. *Phys Rev Lett* 105(15):158101.

20. Mosconi F, Allemand JF, Bensimon D, Croquette V (2009) Measurement of the torque on a single stretched and twisted DNA using magnetic tweezers. *Phys Rev Lett* 102(7):078301.
21. Lipfert J, Kerssemakers JWJ, Jager T, Dekker NH (2010) Magnetic torque tweezers: measuring torsional stiffness in DNA and RecA-DNA filaments. *Nat Methods* 7(12):977–980.
22. Oberstrass FC, Fernandes LE, Bryant Z (2012) Torque measurements reveal sequence-specific cooperative transitions in supercoiled DNA. *Proc Natl Acad Sci USA* 109(16):6106–6111.
23. Forth S, et al. (2008) Abrupt buckling transition observed during the plectoneme formation of individual DNA molecules. *Phys Rev Lett* 100(14):148301.
24. Schöpflin R, Brutzer H, Müller O, Seidel R, Wedemann G (2012) Probing the elasticity of DNA on short length scales by modeling supercoiling under tension. *Biophys J* 103(2):323–330.
25. Moroz JD, Nelson P (1998) Entropic elasticity of twist-storing polymers. *Macromolecules* 31(18):6333–6347.
26. Lipfert J, Wiggin M, Kerssemakers JWJ, Pedaci F, Dekker NH (2011) Freely orbiting magnetic tweezers to directly monitor changes in the twist of nucleic acids. *Nat Commun* 2:439.
27. Wang MD, et al. (1998) Force and velocity measured for single molecules of RNA polymerase. *Science* 282(5390):902–907.
28. Marko JF (2007) Torque and dynamics of linking number relaxation in stretched supercoiled DNA. *Phys Rev E* 76(2 Pt 1):021926.
29. Sheinin MY, Forth S, Marko JF, Wang MD (2011) Underwound DNA under tension: structure, elasticity, and sequence-dependent behaviors. *Phys Rev Lett* 107(10):108102.
30. Allemand JF, Bensimon D, Lavery R, Croquette V (1998) Stretched and overwound DNA forms a Pauling-like structure with exposed bases. *Proc Natl Acad Sci USA* 95(24):14152–14157.
31. Howard J (2001) *Mechanics of Motor Proteins and the Cytoskeleton* (Sinauer Associates, Sunderland, MA).
32. Sternberg SH, Redding S, Jinek M, Greene EC, Doudna JA (2014) DNA interrogation by the CRISPR RNA-guided endonuclease Cas9. *Nature* 507(7490):62–67.
33. Jinek M, et al. (2014) Structures of Cas9 endonucleases reveal RNA-mediated conformational activation. *Science* 343(6176):1247997.
34. Nishimasu H, et al. (2014) Crystal structure of Cas9 in complex with guide RNA and target DNA. *Cell* 156(5):935–949.
35. Wiedenheft B, et al. (2011) Structures of the RNA-guided surveillance complex from a bacterial immune system. *Nature* 477(7365):486–489.
36. Jiang W, Bikard D, Cox D, Zhang F, Marraffini LA (2013) RNA-guided editing of bacterial genomes using CRISPR-Cas systems. *Nat Biotechnol* 31(3):233–239.
37. Jinek M, et al. (2012) A programmable dual-RNA-guided DNA endonuclease in adaptive bacterial immunity. *Science* 337(6096):816–821.

38. Günther K, Mertig M, Seidel R (2010) Mechanical and structural properties of YOYO-1 complexed DNA. *Nucleic Acids Res* 38(19):6526–6532.

39. Lipfert J, Klijnhout S, Dekker NH (2010) Torsional sensing of small-molecule binding using magnetic tweezers. *Nucleic Acids Res* 38(20):7122–7132.

40. Sashital DG, Wiedenheft B, Doudna JA (2012) Mechanism of foreign DNA selection in a bacterial adaptive immune system. *Mol Cell* 46(5):606–615.